ISSN 2278-2540 | DOI: 10.51583EMAS | Volume XV, Issue X, October2026

A Physics-Informed Neural Network (PINN) Framework for Predicting Stress-Dependent Permeability Evolution and Pressure Depletion in Compacting Reservoirs

Jeevana Sasindu Wickramaarachchige[1*], Sachini Dulana Amarasena[2] , Dona Thisari Mahimekhala Iddamalgoda[3], Daim Safeer Mughal[4]

[1]School of Environment and Civil Engineering, Chengdu University of Technology, Chengdu, China

[2]School of Petroleum Engineering, Southwest Petroleum University, Chengdu, China

[3]School of Computer Science & Cyber Security, Chengdu University of Technology, Chengdu, China

[4]School of Management and Economics, Chongqing University of Post and Telecommunications, Chongqing, China

DOI: https://doi.org/10.51583/IJLTEMAS.2026.151000051

Received: 21 October 2026; Accepted: 26 October 2026; Published: 05 November 2026

ABSTRACT

Accurately modeling the coupled hydro-geomechanical behavior of compacting hydrocarbon reservoirs is critical for reliable production forecasting and subsurface management. Traditional numerical simulators, such as finite element and finite difference methods, often suffer from massive computational overheads and complex grid-generation bottlenecks when handling stress-dependent permeability evolution. Conversely, purely data-driven machine learning models frequently fail to respect fundamental physical laws, leading to unphysical predictions and poor extrapolation capabilities. To address these limitations, this paper proposes a physics-informed neural network (PINN) framework explicitly designed to simulate transient pore pressure depletion and stress-dependent permeability degradation in compacting reservoirs. By embedding mass conservation governing equations, exponential permeability constitutive relations, and boundary conditions directly into the neural network's multi-objective loss function, the proposed architecture acts as a continuous, mesh-free surrogate model. Utilizing automatic differentiation to evaluate exact spatial and temporal derivatives, the framework eliminates spatial discretization errors while maintaining strict physical consistency. Furthermore, a staged hybrid optimization strategy combining Adam and L-BFGS algorithms is implemented to navigate the complex optimization landscape. Benchmarking results demonstrate that the proposed PINN framework successfully achieves near-instantaneous surrogate evaluations and significant computational speedups compared to conventional simulators, offering a robust and efficient pathway for real-time reservoir management and subsurface monitoring.

Keywords: Physics-Informed Neural Networks; Stress-Dependent Permeability; Hydro-Poromechanical Coupling; Mesh-Free Surrogate Modeling; Reservoir Simulation.

INTRODUCTION

During the active production life cycle of a hydrocarbon reservoir, the continuous extraction of oil and gas inherently alters the delicate physical state and structural integrity of the geological rock matrix. As production operations are sustained and formation fluids are continuously withdrawn from the subsurface environment, the internal pore fluid pressure inevitably decreases. In a typical deep underground reservoir setting, the total external overburden stress generated by the massive weight of the overlying earth and sedimentary rock layers remains essentially constant throughout the extraction process. According to the fundamental principles of poromechanics, this continuous depletion of internal pore pressure under constant

ISSN 2278-2540 | DOI: 10.51583EMAS | Volume XV, Issue X, October2026

external loading results in a gradual, proportional increase in the net effective stress acting directly on the solid rock skeleton. This fundamental physical relationship implies that as the fluid pressure drops, the solid matrix must bear a progressively larger portion of the immense geological load. Consequently, this escalating effective stress triggers a gradual, yet highly significant, physical alteration in the internal pore structure, heavily influencing the overall volume and transport capabilities of the reservoir rock [1]

This continuous stress alteration and subsequent structural deformation heavily impact specific lithologies and reservoir types. Extensive geological and operational research indicates that many highly productive reservoirs discovered in prominent regions such as the North Sea, the Gulf of Mexico, and offshore zones in Angola and Brazil are primarily situated in unconsolidated sands or weakly consolidated sandstones [2]. These specific geological formations are inherently soft, highly compressible, and therefore exceptionally prone to severe mechanical compaction. Furthermore, pressure depletion associated with sustained hydrocarbon production in these compliant formations may induce large physical strains and irreversible plastic deformations within the reservoir rocks. The consequences of such severe mechanical compaction are often detrimental, potentially leading to macroscopic operational issues such as large-scale surface subsidence, devastating well failures due to casing shear, significant permeability damage, and overall irreversible reservoir impairment [2] .

The mechanical compaction driven by this escalating effective stress severely restricts the ability of reservoir fluids to flow through the porous network. As the rock grains are forced closer together under the increasing load, pore bodies compress, and critical connecting pore throats physically close. Figure 1 shows the microscopic mechanism of stress-dependent pore compaction and capillary bundle deformation under increasing effective stress. Studies extensively note that absolute permeability can change drastically in response to an increase in the effective stress within the rock pore system owing to depressurization during the production life cycle [3]. For specific highly compactable formations, particularly low permeability lithic sandstones, mechanically collapsing chalks, or heavily fractured rock systems, the resulting reduction of absolute permeability can be astonishingly high, sometimes reaching up to 90% of the initial pre-production value [4] . This drastic, non-linear degradation of permeability underscores the absolute necessity of explicitly modeling stress-dependent permeability. Ignoring these dynamic changes and assuming permeability remains a static constant inevitably leads to highly inaccurate production forecasting, severely flawed economic evaluations, and suboptimal field development strategies.

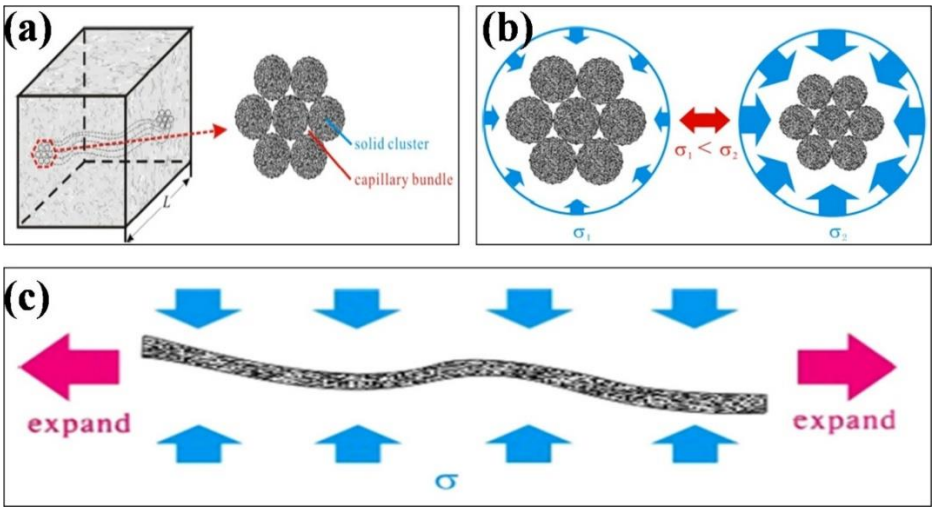


Figure 1:Conceptual model of stress-dependent pore compaction: (a) REV, (b) pore shrinkage, and (c) channel deformation [5].

Accurately modeling these complex, tightly coupled interactions between fluid flow, transient pore pressure, and rock deformation is an incredibly taxing endeavor for traditional numerical simulation techniques. Established computational methods utilized in the petroleum industry, such as the Finite Element Method (FEM) and the Finite Difference Method (FDM), rely heavily on discretizing the continuous spatial domain

ISSN 2278-2540 | DOI: 10.51583EMAS | Volume XV, Issue X, October2026

into vast, intricate computational grids. While these standard mesh-based numerical methods are historically robust and mathematically sound, conventional numerical methods can be exceptionally computationally demanding when applied to complex multiphysics problems within heterogeneous porous media. This specific computational burden becomes particularly prohibitive and entirely impractical for modern real-time analysis applications and rapid decision-making environments[6].

Furthermore, traditional numerical solvers are strictly constrained by their heavy dependency on these localized computational grids. The absolute necessity for high-fidelity mesh generation to capture localized stress concentrations, coupled with the highly complex iterative coupling schemes required to accurately handle the dynamic interaction between stiff soil skeletons and transient fluid flow, often leads to prohibitive computational costs [7]. In practical reservoir management, routine operational workflows such as continuous history-matching, dynamic sensitive analysis, and comprehensive project design optimization fundamentally require multiple simulation runs [8] . Consequently, relying solely on heavy numerical models like FEM or FDM for these large-scale, strongly coupled hydro-mechanical evaluations leads to prohibitively inefficient computations, creating severe workflow bottlenecks [7,8].

To strategically bypass the immense computational expense and time constraints of traditional numerical simulators, engineers and researchers have increasingly turned to deep learning and artificial intelligence. However, the deployment of purely data-driven machine learning models presents critical, inherent limitations when applied to strictly governed physical systems like reservoir simulation. The most prominent issue is the infamous “black box” problem. Traditional artificial neural networks (ANNs) generally fail to fully leverage the implicit physical information contained within the collected engineering data, frequently making the predicted outputs physically inconsistent [9]. Operating entirely as a black box, a purely data-driven model inevitably leads to predictions that may be physically inconsistent or completely implausible when evaluated against established scientific principles [8] .

Moreover, this lack of rigorous physical grounding leads to severe extrapolation failures. Because standard machine learning relies entirely on the interpolative patterns found within the training dataset, one major shortcoming of data-driven machine learning is the fundamental failure to honor any explicit physical relationship between the inputs and the continuous outputs. Consequently, purely data-driven algorithms severely suffer and frequently fail when attempting to extrapolate predictions outside the specific parameters of their original training domain [10] . This fundamental limitation is further exacerbated by the severe data scarcity constraints typical in petroleum engineering. Purely data-driven methods rely heavily on the sheer quantity and the high quality of training samples. Their overall prediction accuracy declines substantially when field data are sparse, noisy, or geographically limited, making them inherently ill-suited for deep underground reservoir applications where high-quality, continuous wellbore data is notoriously expensive and difficult to obtain [11] .

To comprehensively address the severe computational shortcomings of traditional numerical mesh-based simulators and the fundamental physical limitations of purely data-driven machine learning, Physics-Informed Neural Networks (PINNs) have emerged as a revolutionary, hybrid computational solution. PINNs elegantly integrate deterministic, governing physical laws directly into the versatile, high-dimensional flexibility of deep machine learning architectures. Unlike standard models, PINNs proactively incorporate physical knowledge into the network training process. By mathematically utilizing the explicit residuals of governing nonlinear partial differential equations as soft penalty constraints within the objective function, the neural network is meticulously trained with automatic differentiation operating directly on grid data [9]. Ultimately, this framework strategically constrains the neural network to aggressively minimize the PDE residual alongside all specified spatial boundary constraints and temporal initial conditions [12] .

A primary operational advantage of the PINN framework is its inherently mesh-free architecture. It offers a highly robust, mesh-free alternative for solving complex PDE-governed physical problems [7] . It achieves this mathematical feat by converting the traditional numerical problem of directly solving the governing differential equations on a discrete grid into a continuous, global loss function optimization problem [10] . This fundamental computational shift entirely circumvents the massive computational overhead,

ISSN 2278-2540 | DOI: 10.51583EMAS | Volume XV, Issue X, October2026

mathematical instability, and extensive human labor associated with high-fidelity, multidimensional grid generation [7] .

Furthermore, by explicitly embedding the governing PDEs into the training process, PINNs achieve remarkable physical consistency even when operating with significantly less labeled data. They proactively leverage the underlying physical laws and constitutive relations as a powerful, mathematically rigorous regularization mechanism [6] . This integrated physical constraint acts as a powerful scientific prior, actively guiding the optimization landscape. This critical feature allows the computational model to obtain highly reasonable, physically accurate approximations using significantly smaller datasets [13] . It acts as an absolute safeguard, preventing the model from generating the unphysical, chaotic predictions that are notoriously common in standard, unconstrained artificial neural networks.

Once the PINN is fully trained and mathematical optimization is complete, it acts as an incredibly efficient, continuous analytical surrogate model. In highly complex, spatially heterogeneous reservoir engineering workflows, properly trained PINN-based models have been repeatedly demonstrated to function as a forward simulator that is phenomenally faster than the underlying numerical physics-based simulator. Some advanced PINN models have been shown to execute 400,000 times faster than standard simulators, a staggering reduction in computational latency that allows for true near real-time field analysis and highly robust, continuous uncertainty quantification for modern reservoir management [14] . This paper proposes a theoretical PINN framework specifically developed to model stress-dependent permeability evolution and pressure depletion in compacting reservoirs, addressing the critical gap between slow numerical simulators and unphysical machine learning models.

THEORETICAL FORMULATION

Fluid flow in Porous Media

The fundamental macroscopic behavior of single-phase fluid flow within a geological porous medium is primarily governed by the principle of mass conservation. This foundational principle dictates that the rate of mass accumulation within a specific control volume must perfectly equal the net rate of mass flux entering or exiting that volume, alongside any mass added or removed by external sources or sinks. Mathematically, this mass balance is expressed through the continuity equation. The generalized continuity equation for fluid flow in porous rocks relates the temporal variation of fluid mass stored in the pores to the divergence of the fluid mass flux. To describe the actual physical movement of the fluid through the complex interconnected pore spaces of the rock, the continuity equation must be coupled with an appropriate momentum balance relation. In conventional reservoir engineering, the flow of viscous fluids through porous rock is empirically governed by Darcy's law. Darcy's law postulates that the macroscopic seepage velocity of the fluid relative to the solid rock skeleton is directly proportional to the absolute permeability of the rock and the driving pressure gradient, while being inversely proportional to the dynamic viscosity of the fluid [9,15] . When gravity effects are considered negligible for predominantly horizontal flow scenarios, Darcy's velocity vector is simply driven by the localized pressure gradient.

By mathematically substituting Darcy's law into the mass conservation equation, and further incorporating the equations of state that define the compressibility of both the fluid and the rock matrix, a comprehensive governing equation is derived [9]. This combination results in a parabolic partial differential equation that accurately describes the transient diffusion of fluid pressure throughout the reservoir domain over time. For a single-phase fluid scenario, assuming a constant fluid viscosity and incorporating explicit source or sink terms to represent operational wells, the fundamental governing continuity equation is formulated as:

$$\emptyset c_t \frac{\partial P}{\partial t} - \nabla . \left(\frac{k(\sigma')}{\mu} \nabla P \right) = q_w$$

This governing partial differential equation serves as the core physical constraint that the Physics-Informed Neural Network will systematically solve. Fully understanding the coupled hydro-geomechanical system

ISSN 2278-2540 | DOI: 10.51583EMAS | Volume XV, Issue X, October2026

requires a clear definition of its interacting primary variables, which function as critical coefficients and targets within the neural network loss formulation [9,11]. The dynamic state of the physical system is primarily captured by the pore pressure (P), which is the reservoir formation pressure exerted by the fluid constrained within the pore space [9,15] . This pressure serves as the primary latent unknown variable that the neural network aims to continuously predict across the independent temporal coordinate (t) and the extensive spatial domain [11]. The physical properties of the reservoir fluid also play a critical role in this mathematical formulation. Specifically, the fluid viscosity (μ) defines the dynamic internal friction and dictates the physical resistance to flow through the porous geological network [9,15]. Furthermore, external operational conditions are mathematically represented by the source or sink term (q_w). This specific term denotes the volumetric rate of fluid injection or production, mathematically representing the physical presence and operational effect of active wellbores placed within the reservoir boundaries [9,15].

In addition to fluid properties and operational parameters, the petrophysical and geomechanical characteristics of the rock matrix heavily influence the transient flow dynamics. The porosity ($\emptyset$) represents the void fraction of the reservoir rock, defining the specific volume of interconnected pore space available for fluid storage [9,16]. While conventional simplified models often treat porosity as a static constant, the proposed framework acknowledges that it dynamically alters under geomechanical compaction. This elastic volumetric behavior is quantified by the total compressibility (c_t), which is defined as the mathematical sum of the fluid compressibility and the rock matrix compressibility [9]. Total compressibility dictates exactly how much the pore volume and fluid density change in response to pressure fluctuations during transient fluid flow[16]. Finally, the intrinsic ability of the rock to transmit these fluids is characterized by the absolute permeability [17]. In this highly coupled framework, it is explicitly denoted as a stress-dependent permeability function ($k(\sigma')$), rather than a static scalar value. This explicitly indicates that the permeability dynamically degrades as the effective stress (σ') increases due to the progressive depletion of pore pressure and the subsequent structural compaction of the reservoir rock.

Poromechanical Deformation and Effective Stress

The behavior of a hydrocarbon reservoir during the production life cycle is fundamentally a coupled hydro-geomechanical process. As fluids are extracted from the porous medium, the solid rock skeleton continuously responds to the internal fluid pressure fluctuations and the constant external geological loads. This physical response is mathematically governed by the effective stress principle, originally conceptualized by Terzaghi for soil mechanics and subsequently extended by Biot for general poroelastic media. The effective stress principle postulates that the deformation of the rock matrix is not controlled by the absolute total stress, but rather by the net stress transmitted directly through the grain-to-grain contacts of the solid skeleton [18]. In a poroelastic framework, this relationship is mathematically formulated as:

$$\sigma' = \sigma - \alpha P$$

In this governing equation, the total stress (σ) represents the external mechanical load applied to the rock formation. In a typical reservoir setting, this is predominantly the vertical overburden pressure generated by the massive weight of the overlying sedimentary rock layers. The pore pressure (P) is the internal fluid pressure exerted outward by the liquid or gas residing within the void spaces of the rock. The effective stress (σ') is the resulting net geomechanical stress responsible for matrix deformation, pore collapse, and the subsequent alteration of flow properties [18].

A critical component of this formulation is the Biot coefficient (α), a dimensionless poroelastic parameter that quantifies the exact efficiency of the internal pore pressure in counteracting the external total stress. The Biot coefficient is fundamentally determined by the ratio of the drained bulk modulus of the rock frame (K_d) to the intrinsic bulk modulus of the solid mineral grains (K_s), expressed mathematically as $\alpha = 1 - (K_d/K_s)$ [6,18]. For highly compressible or unconsolidated reservoir formations where the bulk rock frame is significantly softer than the individual mineral constituents, the Biot coefficient approaches unity, effectively reducing the formulation to Terzaghi's original classical principle [4,6] .

ISSN 2278-2540 | DOI: 10.51583EMAS | Volume XV, Issue X, October2026

Understanding the dynamic evolution of effective stress is crucial for accurately simulating reservoir depletion. Throughout the production phase, the total overburden stress acting on the reservoir block remains essentially constant, as the physical mass of the overlying earth does not change. Consequently, a continuous decrease in the formation *P* due to fluid withdrawal inherently results in a proportional, dynamic increase in the effective stress exerted directly on the rock matrix [19,20]. This continuous escalation in both vertical and horizontal effective stresses forces the solid rock grains closer together, triggering mechanical compaction [20].

Initially, this poroelastic compaction manifests as a reduction in the bulk volume and the closure of pre-existing micro-fractures [2,18]. However, as depletion continues and the effective stress crosses critical thresholds, the rock may transition into a shear-enhanced compaction regime. This severe state induces irreversible structural damage, including grain crushing and extensive pore collapse [20,21]. The resulting loss of porosity geometrically restricts the pore bodies and pore throats, triggering a drastic and highly non-linear decline in the rock's absolute permeability [20].

The severity of this compaction and the resulting permeability loss are highly dependent on the intrinsic geomechanical properties of the specific reservoir lithology. Sandstone formations generally exhibit significant variations in stiffness and compressibility depending on their mineralogy, sorting, and degree of consolidation [3,20]. Conversely, carbonate formations, such as limestones and chalks, often possess highly complex and heterogeneous microstructures composed of dense calcite grains mixed with microporous aggregates, generally rendering them more compliant and susceptible to severe compaction than typical sandstones [20]. The fundamental geomechanical and petrophysical properties governing this behavior including failure mode, porosity, permeability, Young's modulus, and Poisson's ratio are summarized in Table 1 for various representative rock formations.

Table 1:Summary of geomechanical parameters and initial physical properties of various rock formations.

Material or Rock Type	**Failure Mode**	**Porosity (%)**	**Initial Permeability (m^2)**	**Young's Modulus (MPa)**	**Poisson's Ratio**	**References**
Bakken Shale (Cylindrical real core)	Compressive / Brittleness failure	4.92	6.218×10^{-19}	75850	0.217	[22]
Bakken Shale (Calibrated digital core cylinder)	Compressive failure / Cementation	4.91	6.000×10^{-19}	75280	0.215	[22]
Weakly consolidated sand (Reservoir model)	Shear failure (Mohr-Coulomb)	30	3.0×10^{-13}	3000	0.45	[4]
Shale matrix (Coupled flow-geomechanics model synthetic case)	Poroelastic compression	7	7.895×10^{-19}	3000	0.3	[18]

Stress-Dependent Permeability Model

During the operational life cycle of a hydrocarbon reservoir, the absolute permeability of the rock formation does not remain constant. Instead, it changes dynamically and highly non-linearly primarily due to mechanical compaction driven by continuous alterations in the localized stress state. As pore fluids are progressively withdrawn and the internal pore pressure decreases, the total overburden stress generated by the overlying rock mass remains largely unchanged. According to the effective stress principle discussed in the previous section, this imbalance forces the effective stress acting directly on the solid rock skeleton to

ISSN 2278-2540 | DOI: 10.51583EMAS | Volume XV, Issue X, October2026

increase proportionally [20] . This increased effective stress structurally alters the detailed pore geometry of the reservoir rock [3] . It directly induces the mechanical closure of pre-existing micro-fractures and forces the physical compression of nano-pores, particularly within softer and highly compressible geological materials [18]. As the rock matrix undergoes this severe compaction, the cross-sectional size of pore bodies and connecting throats is significantly reduced. This reduction naturally increases the tortuosity of the flow paths and critically diminishes the overall fluid connectivity [20] .

The resulting decline in absolute permeability is inherently non-linear. During the initial stages of depletion at lower effective stresses, the permeability drops drastically and rapidly due to the immediate closure of existing natural fractures and the swift compaction of the more compliant components of the porous skeleton. However, as the effective stress continues to rise over time, the rock matrix gradually stiffens and structurally approaches its maximum physical compaction limit. Consequently, the rate of permeability decrease begins to slow down and eventually plateaus at higher stress states [23] . To mathematically capture and predict this highly non-linear decline behavior, reservoir engineers and researchers frequently employ an exponential decay model. Figure 2 shows the exponential decline of the permeability ratio against effective stress under various Poisson's ratios, capturing the non-linear degradation behavior. This specific mathematical model structurally assumes that the permeability decreases exponentially as the effective stress increases or, equivalently, as the pore pressure decreases.

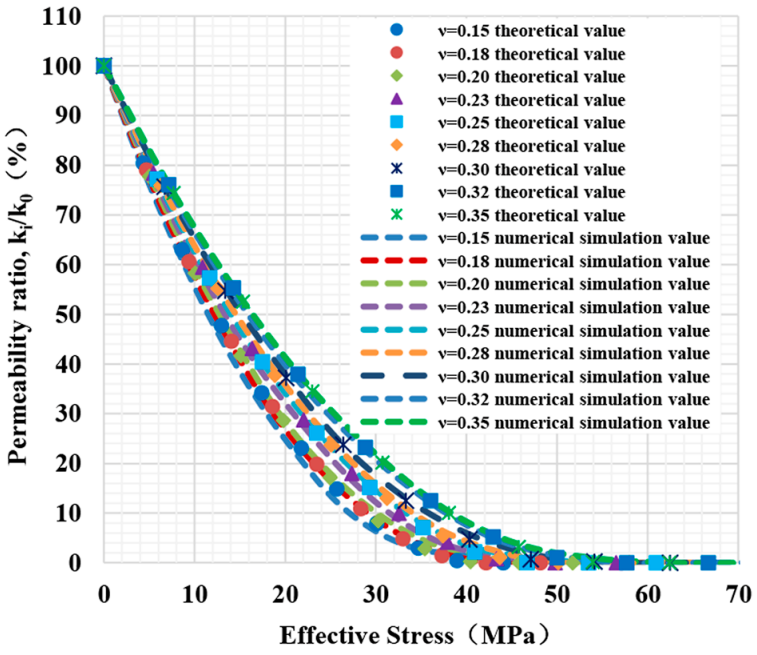


Figure 2:Comparison of theoretical and numerical permeability ratio versus effective stress under various Poisson's ratios [24].

This exponential modeling approach is fundamentally rooted in the concept of the permeability modulus, which dictates the fractional change of permeability in response to a unit change in applied pressure or stress [19,25] . By mathematically integrating this permeability modulus over the stress depletion range, the functional relationship between dynamic permeability and the changing fluid pore pressure can be derived. Depending on the specific geological focus, this exponential correlation can take slightly different but mathematically equivalent forms[23,25]. For the purposes of this proposed framework, the explicit exponential decay model correlating dynamic permeability directly to pore pressure changes is formulated as:

$$k(P) = k_0 \exp[\gamma^*(P - P_0)]$$

where $k(P)$ is the current dynamic permeability, k_0 represents the initial absolute permeability of the undeformed rock, P_0 is the initial baseline reservoir pressure, P is the current transient pore pressure, and γ^* is the defined permeability modulus. This specific modulus (γ^*) acts as a critical stress sensitivity coefficient, governing exactly how rapidly the rock loses its permeability per unit drop in pore pressure.

ISSN 2278-2540 | DOI: 10.51583EMAS | Volume XV, Issue X, October2026

To simulate realistic transient reservoir flow utilizing a Physics-Informed Neural Network, this exponential permeability constitutive relation must be directly incorporated into the macroscopic governing equations. The fundamental physical equation for single-phase fluid flow, as established in Section 2.1, combines mass conservation and Darcy's law [9] . However, because the permeability is now defined as a dynamic exponential function of the local pressure, it is no longer a spatial constant and cannot be linearly pulled outside the differential divergence operator. By substituting the exponential permeability model into the standard fluid flow equation, the system evolves into a highly non-linear partial differential equation. The complete, fully coupled, non-linear governing PDE that the PINN must ultimately solve is formulated as:

$$\phi c_t \frac{\partial P}{\partial t} - \nabla . \left(\frac{k_0 \, exp[\gamma^* (P - P_0)]}{\mu} \nabla P \right) = q_w$$

This mathematical expansion reveals that computing the divergence requires calculating the gradient of the dynamic permeability itself [11,26]. Because the permeability is an exponential function of pressure, this introduces complex products of pressure gradients that tightly couple the fluid flow potential directly with the rock mechanics. Overcoming the stiff non-linearities of this specific coupled equation without requiring a traditional state Jacobian is the primary computational advantage of the proposed PINN methodology [27].

The Physics-Informed Neural Network (Pinn) Framework

Spatiotemporal Neural Network Architecture

The proposed Physics-Informed Neural Network architecture is explicitly designed to model the transient, stress-dependent behavior of a compacting reservoir. Unlike conventional data-driven machine learning models that simply map inputs to outputs based on historical data, the architecture of a PINN is constructed to act as a continuous, mesh-free approximator of the underlying physical fields. In this framework, the continuous spatiotemporal domain serves as the foundation for the network's input layer. To accurately capture the dynamic evolution of reservoir conditions over time and across different geological locations, the input layer directly ingests the Cartesian spatial coordinates (x, y, z) alongside the temporal coordinate (t). This spatiotemporal embedding allows the neural network to evaluate the physical state of the reservoir at any arbitrary point in space and time without being restricted to a fixed computational grid [7,15,28].

The primary objective of this methodological framework is to track the depletion of fluid pressure and the subsequent degradation of permeability due to rock compaction. Therefore, the network is designed to output the surrogate approximations for the latent solutions of the governing partial differential equations. The output layer of the proposed architecture generates two distinct continuous fields. The first output is the predicted pore pressure field ($\hat{P}$), and the second output is the effective stress-adjusted dynamic permeability field ($\hat{k}$). While a single neural network can theoretically output both variables simultaneously, research has demonstrated that utilizing separate networks or a branched-layer topology for different physical variables yields superior performance [29]. This is because pore pressure diffusion is generally a smooth, elliptic process, whereas permeability degradation is a highly localized, stress-dependent process. A branched-layer topology, where a common initial layer diverges into two dedicated branches for pressure and permeability, is therefore proposed to prevent feature interference between these two coupled variables [16,30].

To provide the necessary representational capacity to capture the complex, high-gradient physical phenomena associated with pore collapse and fluid flow, the core of the PINN is built upon a deep Multi-Layer Perceptron (MLP) configuration [31]. The optimal depth and width of the network are crucial for balancing computational efficiency with predictive accuracy. Based on successful implementations in multi-dimensional Darcy flow and hydro-poromechanics, the proposed architecture consists of a deep network ranging from 6 to 12 hidden layers, with a width of 40 to 100 neurons per layer [12,13]. For instance, a configuration of 6 hidden layers with 64 neurons per layer has been shown to effectively handle highly non-linear reservoir simulation tasks [32]. This specific configuration ensures that the network has enough parameters to learn the complex mapping between the spatiotemporal inputs and the stress-dependent outputs.

ISSN 2278-2540 | DOI: 10.51583EMAS | Volume XV, Issue X, October2026

A fundamental requirement of the PINN methodology is the calculation of partial derivatives. The physics-informed loss function, which will be detailed in the subsequent section, relies heavily on Reverse-Mode Automatic Differentiation (AD) to compute the spatial and temporal gradients for the PDE residuals. Consequently, the choice of the activation function within the hidden layers is strictly constrained. The activation function must be smooth and infinitely differentiable to allow for the computation of second-order spatial derivatives required by the fluid flow equations [12,31,33]. The standard Rectified Linear Unit (ReLU) is inherently unsuitable for this architecture because its first derivative is a step function, and its second derivative is zero everywhere except at the origin where it is undefined. This lack of high-order smoothness directly violates the mathematical requirements of the PINN framework and introduces severe artifacts during gradient computation [7,34].

To overcome this limitation, the proposed architecture employs the Hyperbolic Tangent (Tanh) function as the primary activation mechanism across all hidden layers. The Tanh function is infinitely differentiable, making it highly compatible with the automatic differentiation engine [12,15,32]. Alternatively, smoother modern activation functions such as SiLU or Swish are also recommended for this framework. These functions have demonstrated exceptional performance in preventing vanishing gradients while maintaining the strict differentiability required to evaluate complex physical features and enhance the neural network's convergence rate [11,31]. Figure 3 illustrates the comprehensive workflow of the proposed PINN framework, detailing the sequential steps from spatiotemporal input generation and network architecture construction to composite loss evaluation and production forecasting.

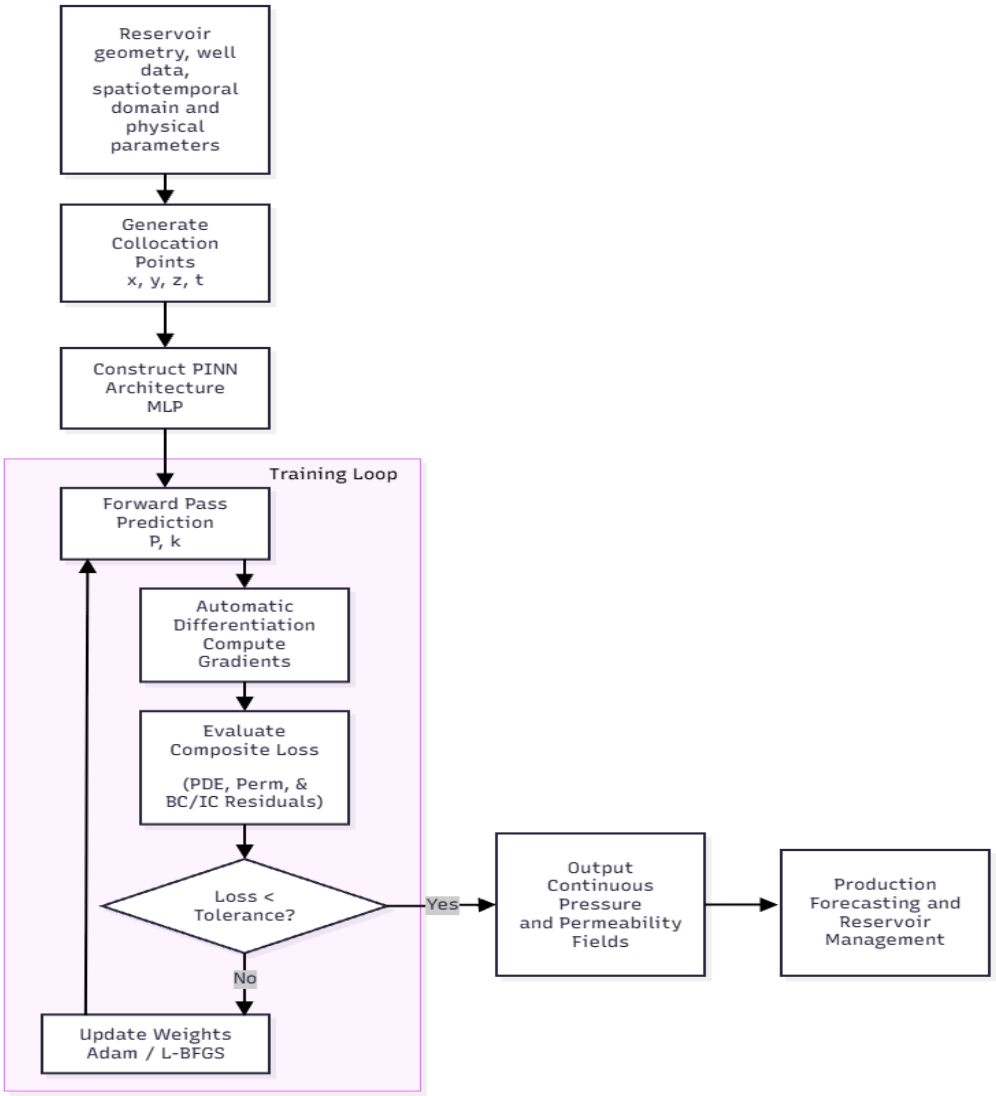


Figure 3:Workflow and architecture of the proposed Physics-Informed Neural Network (PINN) framework for stress-dependent reservoir simulation.

ISSN 2278-2540 | DOI: 10.51583EMAS | Volume XV, Issue X, October2026

Physics-informed loss function formulation

The core innovation of the proposed Physics-Informed Neural Network (PINN) resides in the formulation of a composite loss function. Unlike traditional machine learning paradigms that solely penalize the discrepancy between model outputs and labeled data, the PINN framework integrates the fundamental governing laws of fluid flow and poromechanics directly into the training process. This integration is achieved by transforming the governing Partial Differential Equations (PDEs) into mathematical residual terms. The neural network utilizes AD to accurately compute the required spatial and temporal derivatives of the predicted fields [15,32]. AD employs the chain rule of calculus to evaluate gradients at machine precision, completely avoiding the truncation and rounding error propagation typically associated with numerical finite-difference discretizations [13]. Once these exact derivatives are computed, they are substituted into the governing equations to form continuous residual functions across the spatiotemporal domain [28]. The primary objective of the optimization process is to iteratively adjust the network parameters to drive these residuals as close to zero as possible across a set of densely sampled collocation points.

The primary component of the composite loss function is the PDE loss, which enforces mass conservation and fluid flow kinematics based on Darcy's law. For a single-phase transient flow scenario in a compacting porous medium, the fluid flow residual (r_{flow}) is derived directly from the continuity equation. Specifically, the residual network evaluates the imbalance between the pressure accumulation and the viscous fluid flux. The specific mathematical formulation for the fluid flow residual is defined as:

$$r_{flow} = \varphi c_t \frac{\partial \hat{P}}{\partial t} - \nabla.\left(\frac{\hat{k}}{\mu}\nabla\hat{P}\right) - q_w$$

where $\hat{P}$ represents the predicted pore pressure, $\hat{k}$ is the predicted effective permeability, $\emptyset$ is the porosity, c_t is total compressibility, μ is fluid viscosity, and q_w denotes any source or sink terms [11]. The corresponding loss term, denoted as $Loss_{PDE}$, is subsequently calculated as the Mean Squared Error (MSE) of this fluid flow residual evaluated over all interior domain collocation points [13,32]. Minimizing $Loss_{PDE}$ guarantees that the neural network's predictions physically comply with the principle of mass conservation at every point in space and time.

Beyond standard fluid flow kinematics, accurately modeling compacting reservoirs requires the rigorous enforcement of stress-dependent rock properties. To ensure the neural network obeys complex rock-fluid interactions, physical constraints and constitutive relationships are embedded into the total loss function as secondary penalty terms [27,35] . In this framework, the continuous reduction in permeability driven by increasing effective stress is penalized through a dedicated constitutive residual. The loss equation residual for stress-dependent permeability is formulated as:

$$r_{perm} = \hat{k} - k_0 exp\left[\gamma^*\left(\hat{P} - P_0\right)\right]$$

where k_0 is the initial absolute permeability, P_0 is the initial reservoir pressure, and γ^* is the permeability modulus which defines the sensitivity of the rock to stress changes. This formulation forces the network to dynamically adjust the predicted permeability field ($\hat{k}$) in strict accordance with the localized pressure depletion ($\hat{P}$).

The total composite loss function ($Loss_{Total}$) is constructed by aggregating all individual residual components through a weighted summation. Alongside $Loss_{PDE}$ and $Loss_{Perm}$, the total loss encompasses terms responsible for enforcing the required boundary and initial conditions ($Loss_{BC}$ and $Loss_{IC}$). The training process involves minimizing this composite objective function, thereby ensuring that the resulting surrogate model satisfies the governing PDEs, the stress-dependent constitutive laws, and all domain-specific spatial constraints simultaneously. This holistic physical embedding allows the PINN to generate accurate and physically consistent predictions without relying on conventional mesh-based simulators. Table

ISSN 2278-2540 | DOI: 10.51583EMAS | Volume XV, Issue X, October2026

2 summarizes the individual loss components, mathematical symbols, descriptions, and corresponding references of the composite objective function.

Table 2:Summary of the individual loss components and their descriptions within the composite objective function.

Loss Component	Symbol	Description / What it Penalizes	Reference
Partial Differential Equation Loss	$Loss_{PDE}$	Penalizes residuals of the governing physical/seepage differential equations	[11,27]
Permeability / Data Fidelity Loss	$Loss_{Perm}$	Penalizes discrepancies between network predictions and measured/observed permeability field values or physical rock-model parameters.	[11,36]
Boundary Condition Loss	$Loss_{BC}$	Penalizes deviations from prescribed domain boundaries	[11,27]
Initial Condition Loss	$Loss_{IC}$	Penalizes deviations from baseline reservoir states at time $t = 0$	[11,27]

Initial and Boundary Conditions Enforcement

A critical aspect of developing a robust Physics-Informed Neural Network (PINN) for reservoir simulation is ensuring that the surrogate model adheres strictly to the physical constraints defined by the initial state of the reservoir and its spatial boundaries. In the proposed framework, Initial Conditions (ICs) and Boundary Conditions (BCs) are enforced as "soft constraints" during the optimization process. This implies that rather than hardcoding these conditions directly into the neural network architecture, they are formulated as distinct penalty terms within a composite multi-objective loss function. The neural network learns to satisfy these specific spatiotemporal constraints by minimizing these loss terms concurrently with the Partial Differential Equation (PDE) residual loss over a set of strategically sampled collocation points [31]. Figure 4 illustrates the 2D reservoir domain layout containing a horizontal wellbore and hydraulic fracture, outlining the spatial boundaries for enforcing initial and boundary conditions.

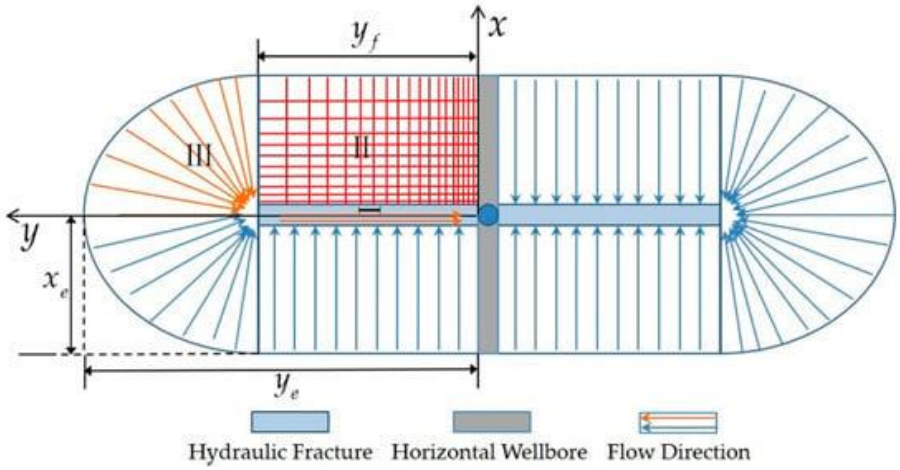


Figure 4:Schematic of the 2D reservoir domain containing a horizontal wellbore and hydraulic fracture, illustrating the spatial boundaries for boundary condition implementations [37].

The initial condition defines the precise state of the reservoir prior to the commencement of any injection or production activities, typically at time $t = 0$. In the context of the proposed single-phase compacting reservoir model, the primary variable of interest is the initial pore fluid pressure distribution across the spatial domain[16]. To enforce this condition, a dedicated set of initial collocation points is sampled

ISSN 2278-2540 | DOI: 10.51583EMAS | Volume XV, Issue X, October2026

exclusively at $t = 0$. The neural network's pressure prediction at these specific coordinates is then compared against the known initial ground-truth values. The initial condition loss, denoted as $Loss_{IC}$, is mathematically formulated as the Mean Squared Error (MSE) between the predicted and true initial states [13]. For a simplified single-phase pressure scenario, this loss term is defined as:

$$Loss_{IC} = \frac{1}{N_{IC}} \sum_{i=1}^{N_{IC}} \left(\hat{P}(x_{i,}0) - P_0(x_i) \right)^2$$

where N_{IC} is the total number of sampled initial points, $\hat{P}(x_i, 0)$ is the network's predicted pressure at spatial coordinate x_i and time $t = 0$, and $P_0(x_i)$ represents the known initial reservoir pressure [11]. Minimizing this term forces the network to accurately replicate the starting conditions before simulating transient flow.

Equally important is the enforcement of physical boundary conditions, which dictate how the fluid interacts with the geometrical limits of the reservoir and the active wellbores. Boundary collocation points are sampled along the domain edges to calculate the boundary loss ($Loss_{BC}$) [15,16]. The proposed framework handles two primary types of boundary conditions. The first type involves constant pressure boundaries, known mathematically as Dirichlet conditions. These are typically applied at active injection or production wellbores where the bottom-hole pressure is maintained at a prescribed constant value [6,38]. The PINN penalizes any deviation of its output from this prescribed value at the specific boundary coordinates. The specific wellbore pressure loss is formulated as:

$$Loss_{Dirichlet} = \frac{1}{N_D} \sum_{i=1}^{N_D} (\hat{P}(x_{D,i}, t) - P_{bc})^2$$

where N_D is the number of Dirichlet boundary points, and P_{bc} is the fixed boundary pressure [39].

The second type of boundary condition governs the outer limits of the reservoir, which are typically modeled as 'no-flow' or closed boundaries. These are classified as Neumann conditions, which impose constraints on the spatial derivative or flux of the pressure variable normal to the boundary [38]. For a closed reservoir boundary, the pressure gradient perpendicular to the boundary must be strictly zero. To enforce this, the PINN utilizes automatic differentiation to compute the spatial gradient of the predicted pressure field at the boundary points and penalizes any deviation from a zero flux state [6,15,16]. The 'no-flow' loss is formulated as:

$$Loss_{Neumann} = \frac{1}{N_N} \sum_{i=1}^{N_N} \left\| \nabla \hat{P}(x_{N,i}, t). \hat{n} \right\|^2$$

where N_N is the number of Neumann boundary points, and $\hat{n}$ is the outward normal vector [15]. By summing $Loss_{Dirichlet}$ and $Loss_{Neumann}$, the total boundary loss $Loss_{BC}$ is constructed, ensuring the network respects the physical confines and operational constraints of the reservoir domain.

Optimization Strategy

The ultimate objective of the Physics-Informed Neural Network (PINN) training process is to discover the optimal set of network parameters, denoted as θ, which consists of all weight matrices and bias vectors across the hidden layers. This is achieved by iteratively minimizing the total composite loss function ($Loss_{Total}$) [13,30]. The optimization relies on a continuous cycle of forward and backward propagation. During the forward pass, the network processes the continuous spatiotemporal inputs to generate the predicted pressure and permeability fields [40]. Subsequently, automatic differentiation and backpropagation are utilized to precisely calculate the gradients of the composite loss function with respect to every individual weight and bias within the network architecture [10,41]. These computed gradients indicate the

ISSN 2278-2540 | DOI: 10.51583EMAS | Volume XV, Issue X, October2026

direction and magnitude of the required parameter adjustments. The parameters are then continuously updated using a chosen gradient-based optimization algorithm, following the fundamental update rule where new weights are calculated by subtracting the product of the learning rate and the loss gradient from the current weights [10].

Training a PINN for coupled hydro-poromechanical problems is notoriously challenging. The process frequently leads to highly non-convex, stiff, and ill-conditioned optimization landscapes. This complexity arises from the necessity to simultaneously minimize multi-objective physics losses, enforce boundary penalties, and match potential data constraints, all of which often possess vastly different physical scales and gradient magnitudes [30,42]. To successfully navigate this complex optimization terrain and ensure robust convergence, the proposed framework employs a sequential, two-stage hybrid optimization strategy.

The first stage of the optimization process utilizes the Adam (Adaptive Moment Estimation) optimizer. Adam is a highly scalable first-order stochastic optimizer that performs an unbiased correction of gradient estimates by calculating both the mean and variance of the gradients to adaptively update the network parameters [30]. Due to its robustness to noisy and unbalanced gradients during the early phases of training, Adam is deployed to perform a comprehensive global search [15,42]. Its primary function is to rapidly navigate the complex loss landscape, forcefully pushing the loss down and preventing the network from becoming permanently trapped in poor local minima [30].

Once the Adam optimizer has located a stable region within the parameter space, the training process transitions to the second stage, which employs the Limited-memory Broyden-Fletcher-Goldfarb-Shanno (L-BFGS) optimizer [12]. L-BFGS is a sophisticated second-order quasi-Newton optimization algorithm [15,31]. While L-BFGS lacks the global search capabilities and scalability of Adam making it highly sensitive to initial starting points and prone to getting stuck if used from scratch, it excels in localized fine-tuning [30]. By leveraging approximate curvature information derived from the Hessian matrix, L-BFGS accelerates local refinement to achieve exact gradient convergence. This second stage is crucial for smoothing out the final physics-informed loss and ensuring the governing differential equations are satisfied with high precision [40,42].

The selection of appropriate neural network hyperparameters is a critical empirical process that balances the model's representational capacity with computational efficiency [12,33]. Based on established benchmarks in reservoir simulation, the proposed architecture recommends deep configurations, typically ranging from 4 to 8 hidden layers, with approximately 20 to 100 neurons per layer depending on the complexity of the domain [12,15,28]. The learning rate for the initial Adam optimization stage is fundamentally set to 10^{-3}, coupled with an exponential or step-decay strategy to maintain exploration early on while allowing for fine-tuning as training progresses [13,15,32,34]. Furthermore, to accommodate the calculation of second-order spatial derivatives via automatic differentiation, piecewise-linear activation functions like standard ReLU are strictly avoided [42]. Instead, the network exclusively utilizes smooth, continuous, and infinitely differentiable activation functions. The Hyperbolic Tangent (Tanh) function serves as the primary standard [12,31,33], while advanced smooth functions such as SiLU or GELU are also highly recommended to prevent vanishing gradients and enhance the overall convergence rate during the rigorous optimization process [11,40]. Table 3 summarizes the recommended neural network hyperparameters, typical ranges, and rationale used in the PINN framework.

Table 3:Summary of recommended neural network hyperparameters and training configurations.

Hyperparameter	**Typical Range / Value**	**Brief Description / Rationale**	**Reference**
Number of Hidden Layers	3-12 layers (typically 4-8)	Controls depth and capacity to represent complex spatiotemporal pressure and displacement fields.	[12,13]
Neurons per Hidden	20 – 256 neurons	Determines layer width, balancing feature	[11,15]

ISSN 2278-2540 | DOI: 10.51583EMAS | Volume XV, Issue X, October2026

Layer	(typically 20-100)	expressivity against computational cost.	
Initial Learning Rate	10^{-3} to 10^{-4}	Sets initial step size for first-order stochastic gradient descent optimizers.	[34,40]
Learning Rate Decay	Exponential / Step Decay (down to 10^{-5})	Gradually reduces step size across epochs to refine convergence near local minima.	[6,8]
Activation Function	Tanh, GELU, ELU, SiLU	Must be continuous and higher-order differentiable (C^2) for AutoDiff	[33,42]
Optimization Strategy	Staged Hybrid: Adam → L-BFGS	Adam performs initial global search; L-BFGS applies 2nd-order curvature updates for exact convergence.	[43,44]
Weight Initialization	Xavier / Glorot (Normal or Uniform)	Maintains stable activation and gradient variance across deep layers at training startup.	[27,28]

PROPOSED IMPLEMENTATION AND BENCHMARKING PROTOCOL

Design of the Synthetic Benchmark Domain

In the absence of physical laboratory core flood measurements or expensive field-scale monitoring datasets, PINN architectures and hybrid surrogate models fundamentally rely on standardized synthetic benchmark domains for numerical verification, forward solver evaluation, and parameter inversion studies [39]. Establishing a mathematically rigorous theoretical domain allows researchers to isolate the computational performance, numerical stability, and convergence behavior of the neural network under controlled boundary and initial conditions [39,45]. For the proposed framework, a standardized two-dimensional synthetic reservoir domain is formulated to evaluate the model's capability in predicting stress-dependent permeability degradation and transient pore pressure diffusion without the confounding effects of severe field-scale geological noise.

The proposed benchmark geometry is structured as a two-dimensional planar reservoir representing a horizontal areal slice of a compacting porous formation [8]. The spatial boundaries are mathematically defined over a continuous computational domain $\Omega = [0, L_x] \times [0, L_y]$ with a uniform formation thickness. To capture localized pressure drawdowns and multi-directional flow gradients effectively, a classic quarter five-spot or two-dimensional square domain configuration is deployed [11]. The outer spatial limits of the domain ($\partial\Omega$) represent impermeable boundaries governed by Neumann no-flow conditions:

$$\nabla P(x,t).\hat{n} = 0 \; on \; (\partial\Omega)$$

where $\hat{n}$ denotes the outward unit normal vector, enforcing complete fluid containment within the reservoir sector [8]. Hydrocarbon production is simulated via an active wellbore situated at specific domain coordinates, operating under a prescribed bottom-hole pressure or a constant volumetric extraction rate [11,27]. This localized sink term introduces steep, non-linear pressure gradients surrounding the wellhead, serving as a rigorous test for the neural network's automatic differentiation capabilities and spatial gradient evaluation [8,9].

The temporal domain for the theoretical benchmark is defined continuously over $t \in [0, T_{max}]$, capturing both early-stage transient fluid diffusion waves and long-term depletion dynamics. Initial conditions across the continuous spatial domain at $t = 0$ specify a uniform baseline reservoir pressure field $P(x, 0) = P_0$. Rather than assuming fixed empirical rock properties, the framework establishes a parametric petrophysical foundation defined by initial absolute permeability, initial porosity, fluid viscosity, and total system compressibility. The geomechanical stress sensitivity is governed by the permeability modulus, which determines the non-linear magnitude of permeability degradation as pore pressure depletes over time [11].

ISSN 2278-2540 | DOI: 10.51583EMAS | Volume XV, Issue X, October2026

To optimize the training of the PINN across complex multi-scale flow features, collocation points are strategically sampled across the continuous spatiotemporal domain $\Omega \times [0, T_{max}]$. Because stress-dependent permeability alterations induce severe non-linear gradients in close proximity to active wellbores, a domain-decomposed non-uniform sampling strategy is recommended. Higher collocation point density is dynamically allocated within the localized wellbore radius to capture steep pressure drawdowns, whereas uniform Sobol or Latin Hypercube sampling is utilized across the far-field interior domain and outer spatial boundaries [9,16]. This adaptive spatial distribution ensures that the PDE residuals and constitutive loss penalties are evaluated effectively across regions exhibiting rapid geomechanical deformation. To guide future numerical implementation and facilitate comparative validation against standard finite-difference or finite-element simulators (e.g., MRST or ECLIPSE), Table 4 summarizes the baseline petrophysical properties, symbols, values, units, and corresponding references for the synthetic benchmark configuration.

Table 4:Summary of baseline parametric variables and properties for the synthetic benchmark setup.

Property	Symbol	Value	Unit	Reference
Initial Absolute Permeability	k_0	1-100	mD	[11,39]
Initial Porosity	φ_0	0.05-0.20	fraction	[11,27]
Fluid Dynamic Viscosity	μ	0.001-0.020	$Pa.s$	[11,27]
Fluid Density	ρ	850-1000	kg/m^3	[11,40]
Total Compressibility	c_t	$1 \times 10^{-9} - 5 \times 10^{-8}$	Pa^{-1}	[11,39]
Initial Reservoir Pressure	P_0	20-30	MPa	[9,11]
Irreducible Water Saturation	S_{wi}	0.10-0.20	fraction	[8,11]

Recommended performance evaluation metrics

To rigorously assess the predictive performance and physical fidelity of the proposed Physics-Informed Neural Network (PINN) framework, a comprehensive benchmarking and error evaluation protocol is established. Because the neural network acts as a continuous mesh-free surrogate model, its spatial and temporal predictions specifically the transient pore pressure and stress-dependent permeability must be directly compared against high-resolution reference solutions generated by conventional numerical simulators, such as fine-grid finite-difference or finite-element solvers [32,40].

To quantify absolute and relative discrepancies across the spatiotemporal domain, standard statistical accuracy metrics are recommended. These include the Root Mean Square Error (RMSE) to measure absolute deviations in physical units [9,40], the Relative L_2 Error to evaluate global dimensionless solution discrepancies independent of physical scaling, and the Coefficient of Determination (R^2score) to quantify the proportion of total variance explained by the neural network model. Table 5 summarizes the mathematical symbols, formulas, descriptions, and corresponding references for the evaluation metrics.

Table 5:Summary of standard statistical error metrics and their mathematical formulations.

Error Metric	Mathematical Symbol / Formula	Brief Description	Reference
Root Mean Square Error	$RMSE = \sqrt{\frac{1}{N}\sum_{i=1}^{N}(y_i - \hat{y}_i)^2}$	Measures the square root of the mean squared difference between predicted and reference values in native physical units.	[11,40]

ISSN 2278-2540 | DOI: 10.51583EMAS | Volume XV, Issue X, October2026

Relative Error	$L_2 = \frac{\lvert\hat{u} - u\rvert_2}{\lvert u\rvert_2} = \frac{\sqrt{\sum_{i=1}^{N}(\hat{u}_i - u_i)^2}}{\sqrt{\sum_{i=1}^{N} u_i^2}}$	Evaluates normalized spatiotemporal solution discrepancies relative to reference magnitude, providing a dimensionless error measure.	[13,32]
Coefficient of Determination	$R^2 = 1 - \frac{\sum_{i=1}^{N}(y_i - \hat{y}_i)^2}{\sum_{i=1}^{N}(y_i - \bar{y})^2}$	Quantifies the proportion of variance in reference data explained by neural network predictions, where values near 1.0 indicate high precision.	[13,32]

In addition to global scalar error metrics, qualitative spatial inspection plays a vital role in verifying model consistency, particularly within high-gradient regions surrounding active wellbores where non-linear permeability degradation is pronounced. Spatiotemporal performance is visualized through side-by-side spatial contour heatmaps comparing reference simulator outputs against PINN predictions on identical colorbar scales, alongside localized absolute error maps and cross-sectional profile cuts. Figure 6 compares the spatial pressure distribution contour heatmaps between the reference simulator, CC-PICNN, and standard PINN models. This dual quantitative-qualitative evaluation protocol ensures that the surrogate model maintains both strict mathematical rigor and physical realism across all production timelines.

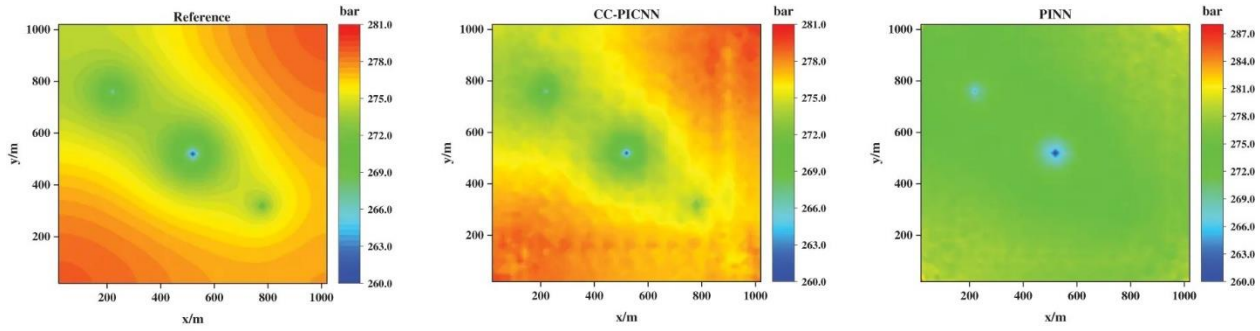


Figure 5:Spatiotemporal comparison of pressure distribution contour heatmaps between the reference numerical simulator, the proposed CC-PICNN, and standard PINN models [46].

DISCUSSION

Computational advantages

The primary computational advantage of the proposed PINN framework lies in its amortization of computational costs through an offline-online training paradigm. Traditional numerical simulation techniques, such as the FEM and FDM, rely heavily on spatial discretization and the continuous assembly and solution of large, sparse systems of linear algebraic equations. For complex hydro-geomechanical processes involving stress-dependent permeability evolution, conventional solvers require iterative numerical schemes and explicit matrix inversions at every discrete time step. This iterative burden leads to substantial computational latency, particularly when evaluating large multi-dimensional domains or executing repeated simulation runs for sensitivity analyses.

In contrast, once the proposed PINN model is fully trained via the multi-objective loss optimization strategy, it operates as a continuous, mesh-free surrogate model capable of near-instantaneous inference [14,29,45] . Because the network directly approximates the governing partial differential equations without requiring mesh generation, pre-processing overheads, or iterative matrix solvers, evaluating new spatiotemporal states requires only a single forward pass [29,45]. Literature and benchmarking studies demonstrate that such physics-informed architectures can achieve dramatic execution speedups often exceeding 400,000 times

ISSN 2278-2540 | DOI: 10.51583EMAS | Volume XV, Issue X, October2026

faster than traditional full-physics numerical simulators in pressure management tasks while maintaining high physical consistency.

This radical reduction in computational latency unlocks critical capabilities for real-time subsurface reservoir management. In practical engineering workflows, tasks such as continuous history-matching, dynamic uncertainty quantification, and Monte Carlo ensemble forecasting require thousands of forward simulations across varied permeability realizations. Traditional numerical solvers render these tasks computationally prohibitive. However, the near-instantaneous evaluation speed of the trained PINN framework allows engineers to perform rapid forward predictions, continuously assimilate live sensor streams from downhole gauges, and support near real-time operational decision-making for compacting reservoirs without encountering severe computational bottlenecks[11,26].

LIMITATIONS OF THE PROPOSED FRAMEWORK

While the proposed Physics-Informed Neural Network framework provides an efficient, mesh-free surrogate approach for modeling stress-dependent permeability evolution and transient pressure depletion, several inherent theoretical limits and simplifying assumptions must be acknowledged. First, the current formulation is established strictly upon a single-phase fluid flow regime. Consequently, it relies on the fundamental assumption that the pore space is occupied by a single, slightly compressible fluid phase with constant or pressure-dependent petrophysical properties. While this single-phase assumption serves as a rigorous baseline for verifying the coupled hydro-geomechanical model, it inherently neglects complex multiphase interactions such as oil, gas, and water co-existence, relative permeability functions, and capillary pressure dynamics typical of mature field operations [16,45]. Furthermore, because single-phase pressure diffusion is governed by parabolic partial differential equations yielding smooth continuous solutions, the current architecture cannot capture hyperbolic shock fronts, moving saturation boundaries, or multi-phase fluid breakthrough phenomena commonly encountered during active waterflooding or gas injection.

Beyond single-phase simplifications, scaling PINN architectures to highly heterogeneous subsurface environments introduce severe training and optimization challenges. In complex geological domains characterized by severe spatial heterogeneity, orders-of-magnitude permeability contrasts, or discrete fracture networks, the loss landscape becomes highly stiff and ill-conditioned. Standard multi-layer perceptrons utilizing smooth activation functions (such as hyperbolic tangents) exhibit an intrinsic spectral bias, making it difficult to resolve sharp spatial gradient jumps across material interfaces without introducing unphysical smoothing artifacts. Additionally, multi-physics formulations that couple transient fluid flow with geomechanical stress equations suffer from gradient pathology. Because the loss gradients governing elastic deformation and fluid diffusion possess vastly different magnitudes, unweighted multi-objective loss functions often lead to optimization stalls or dominance by boundary condition penalties.

To address these current theoretical and computational limitations, future extensions of the framework must incorporate advanced architectural and training paradigms. Promising pathways include domain decomposition strategies to handle complex spatial subdomains, discretization-informed graph neural networks to strictly enforce local flux continuity across heterogeneous grids, and fixed-stress operator-splitting training schemes to decouple stiff multi-physics loss landscapes. Integrating these advanced methodologies will enable the transition of physics-informed surrogate modeling from idealized single-phase benchmarks to robust, full-scale multiphase reservoir simulation environments. Table 6 outlines the current framework limitations, proposed future solutions, and corresponding literature references.

Table 6:Summary of current framework limitations and proposed future solutions.

Current framework Limitation	**Proposed future solution**	**Reference**
Multiphase flow and shock instabilities	Entropy-constrained and conservative PINNs	[6,28]

ISSN 2278-2540 | DOI: 10.51583EMAS | Volume XV, Issue X, October2026

Optimization stiffness and gradient pathology	Adaptive loss weighting and operator-splitting	[7,15]
Geological heterogeneity and property jumps	Domain decomposition and graph neural networks	[8,9]
Near-wellbore gradient smearing	Wellbore domain partitioning and adaptive collocation	[10,27]
High offline training overhead	Transfer learning and operator-learning surrogates	[45,47]

CONCLUSION AND FUTURE OUTLOOK

Conclusion

This paper has presented a rigorous theoretical framework for integrating Physics-Informed Neural Networks (PINNs) into the hydro-geomechanical simulation of compacting hydrocarbon reservoirs. Traditional numerical reservoir simulators, while historically robust, are severely constrained by massive computational overheads, intricate grid-generation requirements, and expensive iterative solvers when handling tightly coupled fluid-rock interactions. Conversely, purely data-driven machine learning models frequently fail due to

their lack of physical grounding, rendering them unreliable for extrapolation outside training regimes. The proposed framework successfully bridges this gap by embedding fundamental governing conservation laws and poromechanical constitutive relations directly into the neural network's optimization pipeline.

The primary theoretical and methodological contribution of this work lies in explicitly formulating and coupling stress-dependent exponential permeability degradation into the physics-informed loss function. Rather than treating absolute permeability as a static petrophysical parameter or relying on decoupled offline approximations, the framework dynamically tracks the non-linear reduction of pore volume and absolute permeability as formation pressure depletes and effective stress increases. By leveraging automatic differentiation to evaluate exact spatial and temporal derivatives at machine precision, the network transforms the traditional discrete grid-solving problem into a continuous loss optimization process. This mesh-free architecture eliminates grid dependency and spatial discretization errors while maintaining strict adherence to mass conservation, initial conditions, and boundary constraints. Ultimately, the methodology establishes a robust mathematical foundation for achieving near-instantaneous surrogate evaluations, providing a powerful pathway to bypass the heavy computational bottlenecks typical of conventional numerical simulators.

Future outlook

Building upon the single-phase theoretical framework established in this study, future research will focus on expanding the methodology toward more complex, multi-physics operational environments. The immediate technical roadmap involves extending the governing equations to account for multiphase fluid flow regimes specifically oil, water, and gas co-existence by integrating fractional flow formulations, relative permeability functions, and capillary pressure relationships into the loss function. To successfully manage the hyperbolic shocks and steep saturation fronts characteristic of multiphase displacement and waterflooding, advanced architectural adaptations such as branched neural topologies and residual-based adaptive collocation resampling will be implemented.

Furthermore, to tackle the optimization stiffness and gradient pathologies associated with heterogeneous subsurface domains containing sharp permeability contrasts or fault networks, future work will integrate domain decomposition strategies and fixed-stress operator-splitting training schemes. Successfully scaling these physics-informed architectures will unlock their ultimate deployment within full-scale digital twin field asset management environments. In such operational setups, the trained surrogate models can

ISSN 2278-2540 | DOI: 10.51583EMAS | Volume XV, Issue X, October2026

continuously assimilate real-time downhole sensor measurements, perform rapid uncertainty quantification and closed-loop history matching, and support proactive, near real-time decision-making for sustainable reservoir management and hazard mitigation.

REFERENCES

1. Wang, H., Ji, B., Lv, C., Zhang, L., Li, X., Cui, C., Yu, H., & Nie, J. (2019). The stress sensitivity of permeability in tight oil reservoirs. *Energy Exploration and Exploitation*, *37*(4), 1364–1376. https://doi.org/10.1177/0144598719855819
2. Nguyen, V. H., Gland, N., Dautriat, J., David, C., Wassermann, J., & Guélard, J. (2014). Compaction, permeability evolution and stress path effects in unconsolidated sand and weakly consolidated sandstone. *International Journal of Rock Mechanics and Mining Sciences*, *67*, 226–239. https://doi.org/10.1016/j.ijrmms.2013.07.001
3. Zhang, H., Liu, H., Luan, G., He, S., Gu, D., Mo, S., & Lei, G. (2014). A novel quantitative petrophysical model for the stress sensitivity of tight sandstones. *Journal of Petroleum Science and Engineering*, *122*, 657–666. https://doi.org/10.1016/j.petrol.2014.09.008
4. Han, G., & Dusseault, M. B. (2003). Description of fluid flow around a wellbore with stress-dependent porosity and permeability. *Journal of Petroleum Science and Engineering*, *40*(1–2), 1–16. https://doi.org/10.1016/S0920-4105(03)00047-0
5. Jiang, G. C., Sheng, K. M., He, Y. B., Yang, L. L., Dong, T. F., Sun, Z., & Jiang, K. L. (2024). Numerical simulation of the temporal and spatial evolution of sandstone pore type reservoir damage types and severity. *Scientific Reports*, *14*(1). https://doi.org/10.1038/s41598-024-76383-0
6. Akhyani, S., Shahbodagh, B., & Khalili, N. (2026). Fully coupled physics-informed neural networks for hydro-mechanical analysis of saturated poroelastic media. *Computers and Geotechnics*, *193*. https://doi.org/10.1016/j.compgeo.2026.107954
7. Cai, E., Gao, Z., Xu, Z., Zuo, S., Wen, M., & Zhang, Y. (2026). A Physics-Informed Deep Learning Framework for Multi-Field Hydro-Mechanical Consolidation Analysis. *International Journal for Numerical and Analytical Methods in Geomechanics*, *50*(7), 3000–3028. https://doi.org/10.1002/nag.70260
8. Han, J. X., Xue, L., Wei, Y. S., Qi, Y. D., Wang, J. L., Liu, Y. T., & Zhang, Y. Q. (2023). Physics-informed neural network-based petroleum reservoir simulation with sparse data using domain decomposition. *Petroleum Science*, *20*(6), 3450–3460. https://doi.org/10.1016/j.petsci.2023.10.019
9. Chen, H. Y., Xue, L., Liu, L., Zou, G. F., Han, J. X., Dong, Y. Bin, Cong, M. Z., Liu, Y. T., & Hosseini-Nasab, S. M. (2025). Physics-informed graph neural network for predicting fluid flow in porous media. *Petroleum Science*, *22*(10), 4240–4253. https://doi.org/10.1016/j.petsci.2025.06.007
10. Badawi, D., & Gildin, E. (2023). *Physics-Informed Neural Network for the Transient Diffusivity Equation in Reservoir Engineering*. http://arxiv.org/abs/2309.17345
11. Zhang, Y., Chen, X., Li, K., & Zou, Y. (2026). A Physics-Informed Neural Network Model for Reservoir Seepage in Porous Media Based on Darcy's Law. *Processes*, *14*(10). https://doi.org/10.3390/pr14101578
12. Almajid, M. M., & Abu-Al-Saud, M. O. (2022). Prediction of porous media fluid flow using physics informed neural networks. *Journal of Petroleum Science and Engineering*, *208*. https://doi.org/10.1016/j.petrol.2021.109205
13. Millevoi, C., Spiezia, N., & Ferronato, M. (2024). On Physics-Informed Neural Networks training for coupled hydro-poromechanical problems. *Journal of Computational Physics*, *516*. https://doi.org/10.1016/j.jcp.2024.113299
14. Ur Rashid, H., Pachalieva, A., & O'Malley, D. (2026). Differentiable multiphase flow model for physics-informed machine learning in reservoir pressure management. *Scientific Reports*, *16*(1). https://doi.org/10.1038/s41598-026-37063-3
15. Haghighat, E., Amini, D., & Juanes, R. (2022). Physics-informed neural network simulation of multiphase poroelasticity using stress-split sequential training. *Computer Methods in Applied Mechanics and Engineering*, *397*. https://doi.org/10.1016/j.cma.2022.115141

ISSN 2278-2540 | DOI: 10.51583EMAS | Volume XV, Issue X, October2026

16. Wahyudi, A., Ariadji, T., Marhaendrajana, T., Sidarto, K. A., & Syihab, Z. (2025). A Fully Implicit Reservoir Simulation Using Physics Informed Neural Networks. *Scientific Contributions Oil and Gas*, *48*(3), 131–147. https://doi.org/10.29017/scog.v48i3.1858
17. Pang, M., Zhang, T., Gao, L., & Qin, B. (2021). Investigating the effects of effective stress on pore-dependent permeability measurements of crushed coal. *PLoS ONE*, *16*(12 December). https://doi.org/10.1371/journal.pone.0261678
18. An, C., Killough, J., & Xia, X. (2021). Investigating the effects of stress creep and effective stress coefficient on stress-dependent permeability measurements of shale rock. *Journal of Petroleum Science and Engineering*, *198*. https://doi.org/10.1016/j.petrol.2020.108155
19. Li, B., Zhou, F., Fan, W., Ren, D., Li, H., & Li, M. (2020). Experimental investigation and theoretical modeling of stress-dependent permeability in naturally fractured tight gas reservoir. *Journal of Petroleum Science and Engineering*, *188*. https://doi.org/10.1016/j.petrol.2020.106949
20. Dautriat, J., Gland, N., Youssef, S., Rosenberg, E., Bekri, S., & Vizika, O. (n.d.). *Stress-Dependent Directional Permeabilities of Two Analog Reservoir Rocks: A Prospective Study on Contribution of m-Tomography and Pore Network Models*.
21. Suri, P., Azeemuddin, M., Zaman, M., Kukreti, A. R., & Roegiers, J.-C. (1997). ENGINEERING Stress-dependent permeability measurement using the oscillating pulse technique. In *Journal of Petroleum Science and Engineering* (Vol. 17).
22. Lin, R., Ren, L., Zhao, J., Tan, X., Rasouli, V., Wang, X., Wu, J., Song, Y., & Shen, C. (2022). Stress and pressure dependent permeability of shale rock: Discrete element method (DEM) simulation on digital core. *Journal of Petroleum Science and Engineering*, *208*. https://doi.org/10.1016/j.petrol.2021.109797
23. Cao, N., Lei, G., Dong, P., Li, H., Wu, Z., & Li, Y. (2019). Stress-Dependent permeability of fractures in tight reservoirs. *Energies*, *12*(1). https://doi.org/10.3390/en12010117
24. Feng, Y., Tang, H., Tang, H., Leng, Y., Shi, X., Liu, J., Wang, Z., & Deng, C. (2023). Influence of geomechanics parameters on stress sensitivity in fractured reservoir. *Frontiers in Earth Science*, *11*. https://doi.org/10.3389/feart.2023.1134260
25. Ali, T. A., & Sheng, J. J. (2015). *SPE-177299-MS Evaluation Of The Effect Of Stress-dependent Permeability On Production Performance in Shale Gas Reservoirs*.
26. An, C., Killough, J., & Mi, L. (2019). Stress-dependent permeability of organic-rich shale reservoirs: Impacts of stress changes and matrix shrinkage. *Journal of Petroleum Science and Engineering*, *172*, 1034–1047. https://doi.org/10.1016/j.petrol.2018.09.011
27. Li, Y., Shen, X., Li, D., Liu, Y., Huang, W., Qiu, J., Yan, X., & Zhang, K. (2026). Two-phase flow simulation in low-permeability heterogeneous reservoirs with a fully implicit scheme-based enriched physics-informed neural network. *Journal of Petroleum Exploration and Production Technology*, *16*(11). https://doi.org/10.1007/s13202-026-02216-7
28. Fuks, O., & Tchelepi, H. A. (2020). LIMITATIONS OF PHYSICS INFORMED MACHINE LEARNING FOR NONLINEAR TWO-PHASE TRANSPORT IN POROUS MEDIA. In *Journal of Machine Learning for Modeling and Computing* (Vol. 1, Number 1). www.begellhouse.com
29. Yuan, R., Huang, X. L., Fang, Y., Kasama, K., Cheng, Y., & He, Y. (2026). A physics-informed machine learning computational framework for solving Mohr-Coulomb plasticity in geomechanics. *Advances in Engineering Software*, *212*. https://doi.org/10.1016/j.advengsoft.2025.104061
30. Xing, H., Yao, G., Yuan, H., Zhao, J., & Wen, D. (2025). Physics-Informed Neural Networks for Solving Parameterized Dual-Domain Darcy–Brinkman Flows in Gradient Porous Mediums. *International Journal for Numerical Methods in Engineering*, *126*(16). https://doi.org/10.1002/nme.70110
31. Cuomo, S., Di Cola, V. S., Giampaolo, F., Rozza, G., Raissi, M., & Piccialli, F. (2022). Scientific Machine Learning Through Physics–Informed Neural Networks: Where we are and What's Next. *Journal of Scientific Computing*, *92*. https://doi.org/10.1007/s10915-022-01939-z
32. Meng, X., Liu, X., Zhang, H., Guo, X., Wang, Y., & Jeng, D. S. (2026). A physics-informed neural network framework for wave-induced dynamic response in a poroelastic seabed. *Computers and Geotechnics*, *198*. https://doi.org/10.1016/j.compgeo.2026.108250

ISSN 2278-2540 | DOI: 10.51583EMAS | Volume XV, Issue X, October2026

33. Tartakovsky, A. M., Marrero, C. O., Perdikaris, P., Tartakovsky, G. D., & Barajas-Solano, D. (2020). Physics-Informed Deep Neural Networks for Learning Parameters and Constitutive Relationships in Subsurface Flow Problems. *Water Resources Research*, *56*(5). https://doi.org/10.1029/2019WR026731
34. Ji, Y., Peng, Y., Wang, X., Chen, Z., & Wu, K. (2026). Physics-Informed Neural Networks for Near-Wellbore Stress Field Prediction with Enhanced Generalization. *Processes*, *14*(14). https://doi.org/10.3390/pr14142254
35. Wang, S., Zhang, S., Xiao, T., Ren, W., Zhang, L., & Tian, Y. (2026). Physics-informed neural networks for predicting the coupled hydro-mechanical behaviour of partially saturated soils. *Georisk*. https://doi.org/10.1080/17499518.2026.2643668
36. Bodong, Z., Maojin, T., Guohua, Z., & Chenglin, L. (2026). An Integrating Physics-Informed Neural Networks and Attention Mechanism based Intelligent Permeability Prediction Method for Shale Reservoirs. In *SPE Journal*.
37. Xiong, S., Liu, S., Weng, D., Shen, R., Yu, J., Yan, X., He, Y., & Chu, S. (2022). A Fractional Step Method to Solve Productivity Model of Horizontal Wells Based on Heterogeneous Structure of Fracture Network. *Energies*, *15*(11). https://doi.org/10.3390/en15113907
38. Ishitsuka, K., & Lin, W. (2023). Physics-informed neural network for inverse modeling of natural-state geothermal systems. *Applied Energy*, *337*. https://doi.org/10.1016/j.apenergy.2023.120855
39. Zhang, Z. (2022). A physics-informed deep convolutional neural network for simulating and predicting transient Darcy flows in heterogeneous reservoirs without labeled data. *Journal of Petroleum Science and Engineering*, *211*. https://doi.org/10.1016/j.petrol.2022.110179
40. Aziz, Md. A., Strauss, T., Mohebujjaman, M., & Khan, T. (2025). *Self-adaptive physics-informed neural network for forward and inverse problems in heterogeneous porous flow*. http://arxiv.org/abs/2512.14610
41. Kalule, R., Abderrahmane, H. A., Ahmed, S., Alameri, W., & Al-Shalabi, E. W. (2026). Relative permeability and capillary pressure estimation via physics-informed machine learning and reinforcement learning. *Petroleum*, *12*(3), 430–443. https://doi.org/10.1016/j.petlm.2026.04.005
42. Liu, Y., & Arson, C. (2026). A Physics-Informed Neural Network for Pressurized Cavities of Arbitrary Shape in Heterogeneous Rock. *Rock Mechanics and Rock Engineering*. https://doi.org/10.1007/s00603-026-05882-5
43. Raissi, M., Perdikaris, P., & Karniadakis, G. E. (2017). *Physics Informed Deep Learning (Part I): Data-driven Solutions of Nonlinear Partial Differential Equations*. http://arxiv.org/abs/1711.10561
44. Cai, M., Gu, H., Hong, P., & Li, J. (2023). A combination of physics-informed neural networks with the fixed-stress splitting iteration for solving Biot's model. *Frontiers in Applied Mathematics and Statistics*, *9*. https://doi.org/10.3389/fams.2023.1206500
45. Samarkanov, O. L., Riazi, M., Irawan, S., & Kamrava, S. (2026). Applications of physics-informed neural networks in fluid flow in porous media - A review study. In *Energy and AI* (Vol. 24). Elsevier B.V. https://doi.org/10.1016/j.egyai.2026.100747
46. Han, J., Xue, L., Jia, Y., Mwasamwasa, M. S., Nanguka, F., Sangweni, C., Liu, H., & Li, Q. (2024). Prediction of Porous Media Fluid Flow with Spatial Heterogeneity Using Criss-Cross Physics-Informed Convolutional Neural Networks. *CMES - Computer Modeling in Engineering and Sciences*, *138*(2), 1323–1340. https://doi.org/10.32604/cmes.2023.031093
47. Pachalieva, A., O'Malley, D., Harp, D. R., & Viswanathan, H. (2022). Physics-informed machine learning with differentiable programming for heterogeneous underground reservoir pressure management. *Scientific Reports*, *12*(1). https://doi.org/10.1038/s41598-022-22832-7